International Journal of Heat and Mass Transfer 127 (2018) 1188–1196

Contents lists available at ScienceDirect

International Journal of Heat and Mass Transfer

journal homepage: www.elsevier.com/locate/ijhmt

Boiling performance on surfaces with capillary-length-spaced one- and two-dimensional laser-textured patterns

Jure Voglar *, Peter Gregorčič, Matevž Zupančič, Iztok Golobič

Faculty of Mechanical Engineering, University of Ljubljana, Askerceva 6, SI-1000 Ljubljana, Slovenia

ARTICLE INFO

Article history:
Received 29 March 2018
Received in revised form 6 June 2018
Accepted 10 July 2018

Keywords:
Capillary length
Laser surface engineering
Micro cavities
Nucleation sites
Pool boiling

ABSTRACT

This investigation used laser-processed 25-μm-thick stainless steel foils as heaters in pool boiling experiments under subcooled and saturated conditions at atmospheric pressure. Boling surfaces were modified by a nanosecond fiber laser. In most cases, laser-textured parts on boiling surfaces were spaced apart by a capillary length of water (2.5 mm) and had different shapes and arrangements. Multi-scale micro-cavities (with diameters ranging from 0.2 to 10 μm) on the laser-textured areas of the surfaces provided potential active nucleation sites. The highest heat flux measured before the burnout was observed on the fully treated sample; this heat flux was a factor of 3.7 greater than that of the untreated sample. The sample with hexagonally arranged textured circular shapes with a diameter of 2.0 mm provided a more than 4-fold higher heat transfer coefficient compared to the untreated sample. All of the laser-textured boiling surfaces showed enhanced pool boiling heat transfer performance in comparison to the untreated surface. The optimal spacing between the laser-textured regions was experimentally found to be equal to the capillary length of the working fluid. Our results demonstrate that laser texturing has strong potential for producing patterned surfaces for engineering applications of boiling heat transfer.

1. Introduction

Nucleate pool boiling is one of the most intensive among all of the heat transfer processes that can be controllably applied in many fields of engineering. Boiling is exploited in electrical power plants [1], dissipation of heat from microelectronic components [2] located in small devices, generation of industrial steam and many other fields [3]. Therefore, advances in boiling heat transfer could accelerate the technological progress of our modern society.

During nucleate boiling, a bubble nucleates and grows from a single site on the heated surface. Formation and subsequent growth of the bubble extracts large quantities of heat via evaporative phase change of the working fluid. When a bubble grows to a certain size, it will depart from the heater surface into the liquid as a result of such factors as the joint effects of surface tension, buoyancy, and inertia. The size and frequency of the departing bubbles along with nucleation site density are among the main parameters affecting the boiling performance of the system. The boiling performance of the heater surface immersed in a working fluid is conventionally depicted with boiling curves, the values of the heat transfer coefficient (HTC) and the critical heat flux (CHF), which is the upper limit of the nucleate boiling regime [4,5]. A complementary approach to presenting the boiling performance of the heater surface is the use of the heater wall-temperature distributions [6], which can be constructed after measurement of the transient temperature field of the heater. Modification of the properties of the heater surface affects the phenomena (e.g., bubble growth) during boiling that can consequently enhance boiling heat transfer [7–9].

Several of the researchers studying the boiling process concentrated their investigation on the changes of wettability with alteration of the surface chemistry and/or topography. For example, enhanced boiling heat transfer on wettability patterned or biphilic surfaces has been reported [7,10–14]. Moreover, the contact angle itself was not found to be a sufficient parameter to predict boiling behaviour [15]. It was found that micro(μ)-cavities and μ -porosity play a crucial role in the boiling performance [8], as explained by Hsu's nucleation criterion [16]. The texture of the boiling surface therefore has a more profound effect on its boiling performance than the contact angle, as was experimentally shown by boiling experiments conducted on textured heater surfaces [17–20].

Rahman et al. [21] observed enhanced boiling heat transfer using surfaces with in-plane variations in substrate thermal conductivity; such surfaces are the so-called "bi-conductive" surfaces. Spatial variations in the surface temperature occurred during

* Corresponding author.
E-mail address: jure.voglar@fs.uni-lj.si (J. Voglar).

https://doi.org/10.1016/j.ijheatmasstransfer.2018.07.056
0017-9310/

boiling, and by tuning the wavelength of these variations to coincide with the capillary length, increases in HTC and CHF of greater than a factor of 5× and 2×, respectively, were shown.

The capillary length λ_c is the characteristic length scale of an interface subject to both surface tension and gravitational forces [21]; for a bubble, the capillary length is defined as

$$\lambda_c = \sqrt{\frac{\sigma}{g\,(\rho_l - \rho_v)}}, \tag{1}$$

where σ denotes the surface tension at the interface of saturated water and water vapour at atmospheric pressure and is equal to 58.9 mN/m, g is the acceleration of gravity (9.81 m/s^2), and ρ_l and ρ_v denote the densities of saturated liquid (957.9 kg/m^3) and vapour (0.596 kg/m^3), respectively. The capillary length for a bubble of water vapour surrounded by saturated liquid water at atmospheric pressure is equal to 2.5 mm.

The work of Rahman et al. [21] inspired us to investigate the boiling performance of surfaces with patterns of active nucleation sites that are spaced by a capillary length in one- or two-dimensional arrangements. In our investigation, the nucleation sites were provided by laser-induced μ -cavities, as previously reported by Gregorčič et al. [8]. Our paper provides a detailed explanation of the local phenomena affecting the overall boiling performance of the heater surfaces.

2. Materials and methods

2.1. Design and fabrication of the boiling surfaces

The boiling surfaces were designed with notion of the optimal wavelength (spacing, A in Fig. 1), as observed by Rahman et al. [21], set equal to the capillary length (2.5 mm). Instead of testing only a one-dimensional pattern (as in Ref. [21]), we tested two other two-dimensional wettability pattern designs (Fig. 1). The spacing length (A) for most of the cases was kept at 2.5 mm, and the pattern features length (dimension B in Fig. 1) was varied over three different values (0.5 mm, 1.0 mm and 2.0 mm) to determine the most favourable coverage of laser-textured parts of the boiling surface (Table 1). The two-dimensional designs were expected to perform better than the one-dimensional ones because prevention of bubble coalescence and possible dry-outs of the surface should be improved in the two-dimensional cases.

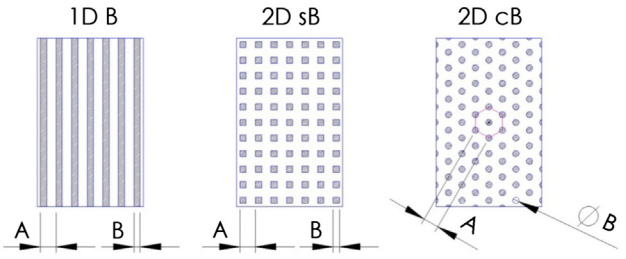

Fig. 1. Drawing of three different designs for the boiling surface: parallel lines (1D), squares (2D s) and circles (2D c); dimensions: A = 2.5 mm and B = 1.0 mm; hatched areas indicate laser-textured regions (with active nucleation sites).

Table 1
Coverage of laser-textured parts (%) of the patterned boiling surfaces.

Pattern\B [mm]	0.5	1.0	2.0
1D	20.0	40.0	80.0
2D s	4.0	16.0	64.0
2D c	1.8	7.3	29.0

Different boiling surface designs were made on 25-μm-thick AISI 316 (EN 1.4401, ISO X5CrNiMo17-12-2) stainless steel foil (Precision Brand). The μ -cavities (active nucleation sites) were produced by using laser surface texturing in a similar manner as described in [8]. A nanosecond fiber laser (SPI Lasers, Ltd., G4, SP-020P-A-HS-S-A-Y) with a wavelength of 1060 nm, pulse duration of 28 ns at full width at half maximum, average power of 3.81 W and pulse frequency of 25 kHz was used to induce μ -cavities. These μ -cavities appear because a laser beam having a 0.03-mm beam waist diameter was directed by a scanner (Raylase, SS-IIE-10) across the surface at the velocity of 150 mm s^{-1}; the scanning lines were separated by alternating values of Δy = {60, 65, 70} μm. The processed surface was placed in a focal position. In this study, the laser-surface interaction leads to modification of both the surface chemistry and topography which, in fact, contribute to changes in the wettability of the surface [22].

2.2. Experimental apparatus

The experimental apparatus for testing of the boiling performance on different thin metal-foil heater samples is shown in Fig. 2. A heating foil with boiling-surface dimensions of 27 mm × 17 mm was supplied with DC power to use Joule heating to supply heat. The supplied heat was transferred to the working fluid inside the boiling chamber. The DC power was controlled using a programmable AC-DC convertor (TDK Lambda GEN 10-1000). The temperature of the bulk liquid was monitored using a calibrated Class 1 type-K thermocouple. The supplied heating power was calculated by measuring the voltage drop and current across the thin metal-foil test sample using a current-measuring circuit with a shunt resistor (Empro LAB-250–100). The temperature field of the bottom side of the heating foil (covered with high emissivity paint) was recorded using an IR camera (FLIR SC6000) at a sampling frequency of 1000 Hz and a resolution of 150 μm per pixel. Use of infrared thermography to measure transient temperature field of heater during boiling experiments is relatively common practice amongst researchers of the boiling phenomenon [23–25]. Bubble dynamics in visual spectra were also observed from the side using a high-speed camera (Photron UX100). Vapour condensed back to liquid inside the water-cooled coil reflux condenser placed above the boiling chamber.

Prior to performing the boiling experiments, the IR camera was calibrated over the range of 80–180 °C in increments of 5 K. The expanded absolute measurement uncertainty of the temperature measurement was determined to be 2 K, which was constant over the entire calibration range. The expanded relative measurement uncertainty of the input heat flux is nearly constant within the entire measurement range and is equal to approximately 0.5% of the measured value.

The boiling experiments were conducted at atmospheric pressure using re-distilled water as the working fluid (Roth 3478.2), which was degassed by boiling for one hour before the measurements. An auxiliary heater was used for preheating and for maintaining the saturation temperature of the liquid. During the actual measurement, at a given heat flux, the auxiliary heater was turned off and therefore did not influence the flow regime inside the working fluid. Each individual foil sample was measured in subcooled (10 K of subcooling; heat flux up to 125 kW/m^2) and saturated boiling conditions (up to burnout). Between the measurements, auxiliary heater was turned on for 30 min to sustain the desired temperature of the bulk liquid.

2.3. Temperature field analysis

Analysis of the transient temperature field of the heater started by merging all the temperature values of the IR thermographic

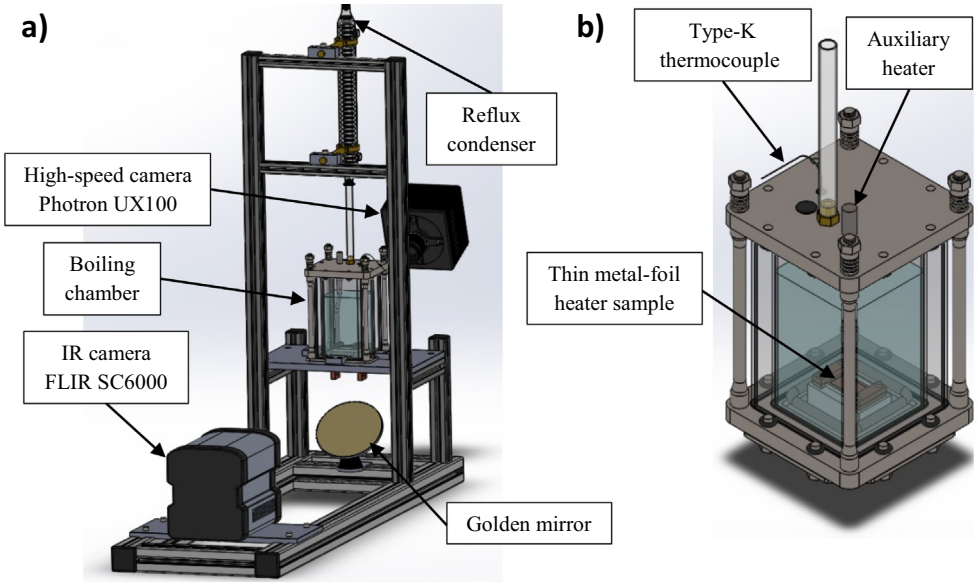

Fig. 2. Schematic presentation of the (a) pool boiling experimental apparatus and (b) boiling chamber.

recordings obtained at certain heat flux into a single vector. The 10-second IR camera recordings captured during nucleate boiling (10,000 individual frames) were of size of 100 by 50 points (5000 pixels), corresponding to 50 million individual values of temperature readings. The wall-temperature vectors contain and merge local and temporal information of the measured temperature field.

The wall-temperature vectors at each heat flux were visually presented using a statistical approach. The heater wall-temperature distributions were constructed by the calculating probability density of each wall-temperature vector. The probability density p of measured variable with population size N can be calculated as follows:

$$p_i = \frac{n_i}{N\,b}, \tag{2}$$

where i is the current bin number, n_i is the number of its elements and b is the bin width. To obtain representative heater wall-temperature distributions, we took into account all the acquired data (10 s of recording), and the temperature range was divided into 50 equidistant bins in all cases. Note that the bin width (b) has units of K; therefore, the probability density has units of K^{-1}.

3. Results and discussion

3.1. Surface characterization

Both bare and laser-textured surfaces were characterized by measuring the apparent (static) contact angle and roughness. The morphology and micro-size features of laser-textured surface were observed using a scanning electron microscope (SEM; JEOL JSM-6500F at 15 kV). SEM micrographs of laser-induced active nucleation sites are shown in Fig. 3. Parallel lines of the laser ablation treatment are shown in Fig. 3(a), and multi-scale μ -cavities (with diameters from 0.2 to 10 μm) are found in Fig. 3(b–c).

The surface roughness measurements of bare and treated samples were performed using a Mitutoyo SJ-301 portable surface roughness tester. The roughness measurements were conducted with the cutoff wavelength of 0.25 mm and 0.80 mm for bare and treated samples, respectively. The sampling length was 3 mm in all cases. Table 2 includes four roughness parameters R_a, R_y, R_z and R_q, each of which was calculated as an average value from 6 measurements (3 along and 3 perpendicular to the sample's length). Table 1 also includes the values of the apparent (static)

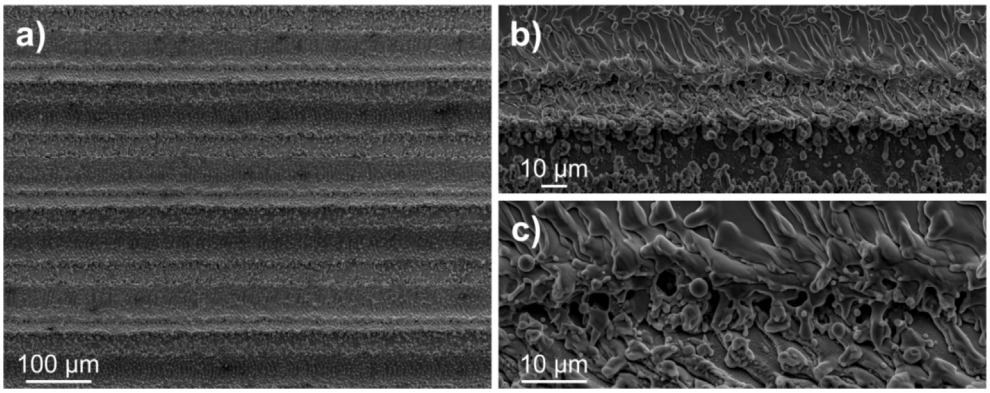

Fig. 3. SEM images of the treated part of 25-μm thick SAE 316 stainless steel foil.

Table 2
Surface roughness parameters and static contact angle.

Foil sample	R_a [μm]	R_y [μm]	R_z [μm]	R_q [μm]	θ [°]
Bare	0.16	0.81	0.64	0.20	80.1
Treated	2.10	9.57	8.28	2.43	0.0

contact angle (θ). The contact angle was measured using an optical tensiometer at room temperature (22 °C) and a 50 μL drop of distilled water.

All of the measured surface roughness parameters are approximately one order of magnitude larger for the treated parts of the boiling surface in comparison to the untreated (bare) surface (Table 2). The static contact angle on untreated surface is equal to 80 ± 3°; immediately after laser processing, the surfaces are in a saturated Wenzel regime with a static contact angle of 0° [26]. Similar results after laser texturing of the stainless steel were observed elsewhere [22]. However, as already shown [22], the contact angle increases over time if the laser-textured metal surface is exposed to atmospheric air. We performed the boiling experiments one week after texturing; at that time, the static contact angle was less than 39°. However, it was shown [8,27–29] that in the case of surfaces covered by multi-scale μ -cavities, the boiling performance does not (strongly) depend on wettability because the wettability just shifts the required range of the μ -cavities' diameters [15]. This was also the primary reason that we decided to produce the active nucleation sites by using the described laser-texturing method.

3.2. Boiling performance

The classical approach for assessment of the boiling performance was employed first. Boiling curves were constructed after measurement of the heat flux and the average superheating above the bulk liquid temperature. The boiling curves (Fig. 4) indicate that the tested surfaces exhibited similar boiling performance in both saturated and subcooled conditions. The lowest heat transfer coefficient was measured on the bare (untreated) stainless steel sample, where part of the boiling curve has a negative slope (at heat fluxes higher than 125 kW/m^2), as experimentally observed in previous studies [30]. During the saturated experiment [Fig. 4 (b)], the best boiling performance at the low heat flux range (up to 400 kW/m^2) is provided by sample 1D 2.0, and for higher heat flux operation (400 kW/m^2 or higher), the 2D c2.0 sample provided the highest heat transfer coefficient (up to 54.6 kW/m^2 K).

The highest achieved values of heat flux in saturated pool boiling experiments were in most cases well below Zuber's theoretical limit [31]. This finding was also observed according to previous measurements on thin metallic heaters [15]. The primary reason for this observation is small foil thickness in combination with its thermal effusivity that causes burnout to occur at heat flux lower than the theoretical limit predicted by Zuber. Asymptotic heater thickness [32], above which the heater thickness does not significantly affect the CHF value, in the case of AISI 316 stainless steel is equal to 845 μm, which is significantly thicker than the foils used in our experiments (25 μm).

The highest measured heat flux before burnout was 325 kW/m^2 for the bare and 1200 kW/m^2 for the fully treated sample. The average HTC in the entire measured range during saturated pool boiling was 9.1 kW/m^2 K and 33.5 kW/m^2 K for the bare and the treated sample, respectively. The values of the maximal measured heat flux and the average HTC for other tested foil samples are presented in Table 3.

It can be seen that the highest measured heat flux monotonically increases with increasing share of the treated surface (B). This increase is also observed for the value of average HTC with one exception (2D s2.0). We can observe that all of the patterned surfaces caused increases in the maximal/burnout heat flux and the HTC. Therefore, the use of laser-textured patterned boiling surfaces enhanced the nucleate boiling heat transfer. The fully treated boiling surface exhibited the largest burnout heat flux of 1200 kW/m^2, which is near the theoretical CHF limit proposed by Zuber [31]. The highest achieved average HTC was observed for the 2D c2.0 sample, followed by the 1D 2.0 sample and the fully treated samples. The boiling performances of two-dimensional pattern designs are not found to be better than those of their one-dimensional counterparts in all cases as expected before. The right combination of arrangement and size of the textured areas is the key factor for achieving high HTC values.

The heat transfer coefficient is in general increasing with increasing heat flux; therefore, the samples that achieved higher

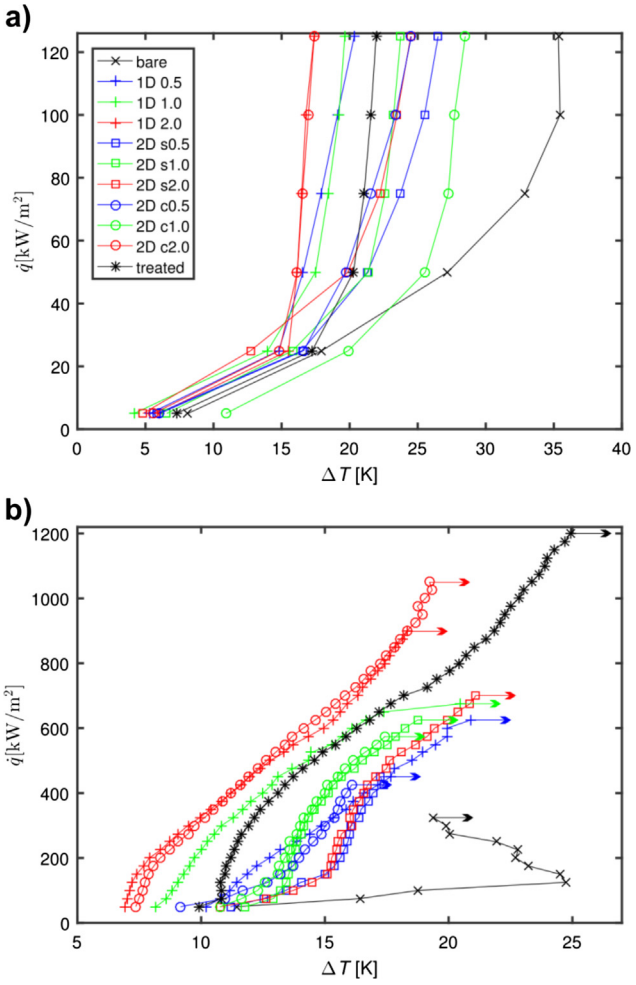

Fig. 4. Boiling curves at subcooled (a) and saturated (b) pool boiling on laser-textured, patterned surfaces with feature spacing equal to the capillary length (A = 2.5 mm; arrows indicate burnout).

Table 3
Maximal measured heat flux (kW/m^2) and average HTC in brackets (kW/m^2 K) on laser-textured patterned surfaces in saturated conditions.

Pattern\B [mm]	0.5	1.0	2.0
1D	625 (20.3)	675 (27.3)	900 (34.9)
2D s	450 (15.6)	625 (21.5)	700 (21.2)
2D c	425 (16.2)	575 (20.9)	1050 (37.5)

burnout heat flux could have a higher value of the average HTC (Table 3). For better comparison of the boiling performance of the tested samples, the HTC enhancement factor was calculated for all of the samples in the heat flux range up to 325 kW/m^2. The HTC enhancement factor was calculated as the ratio between the average HTC (up to 325 kW/m^2) and the average HTC on the bare sample. The values of the HTC enhancement factor are presented in Table 4. The fully treated sample has the HTC enhancement factor of 1.82. The trend observed in Table 4 are the same as that in Table 3 and, therefore, additionally confirm that use of average HTC in Table 3 is appropriate for comparison of the boiling performance of the tested samples.

Table 4
HTC enhancement factor on laser-textured patterned boiling surfaces in saturated conditions.

Pattern \B [mm]	0.5	1.0	2.0
1D	1.56	2.07	2.47
2D s	1.35	1.50	1.36
2D c	1.49	1.55	2.36

Fig. 5 shows wall-temperature distributions during saturated pool boiling that were calculated for the bare sample and for the samples with highest HTC enhancements for each of the boiling surface designs (1D, 2D s and 2D; see Table 4). The general trend of lowering and the right shift of the main peaks with increasing heat flux could be observed in nearly all of the cases [black arrow in Fig. 5(b)]. The bare and the 2D 1.0 sample show significantly larger population of temperatures near the saturation temperature compared with the other tested samples. This finding could be attributed to presence of larger bubbles with lower nucleation frequency (compared to 1D 2.0 and 2D c2.0 samples), as confirmed by the results in Fig. 8(a). The standard deviation (σ) of heater wall-temperatures [Fig. 5(e)] generally increases with increasing heat flux and reach the highest value (considering the entire range) for the bare sample. This finding indicates that untreated sample requires greater superheating for bubble activation because of the lack of μ-cavities and - at the same time - produces relatively larger bubbles with contact diameters of up to several millimetres. In contrast, in the laser-textured areas the average bubble contact diameter is below 1 mm, and the bubble departure frequencies (Fig. 8), as well as nucleation site densities, were significantly

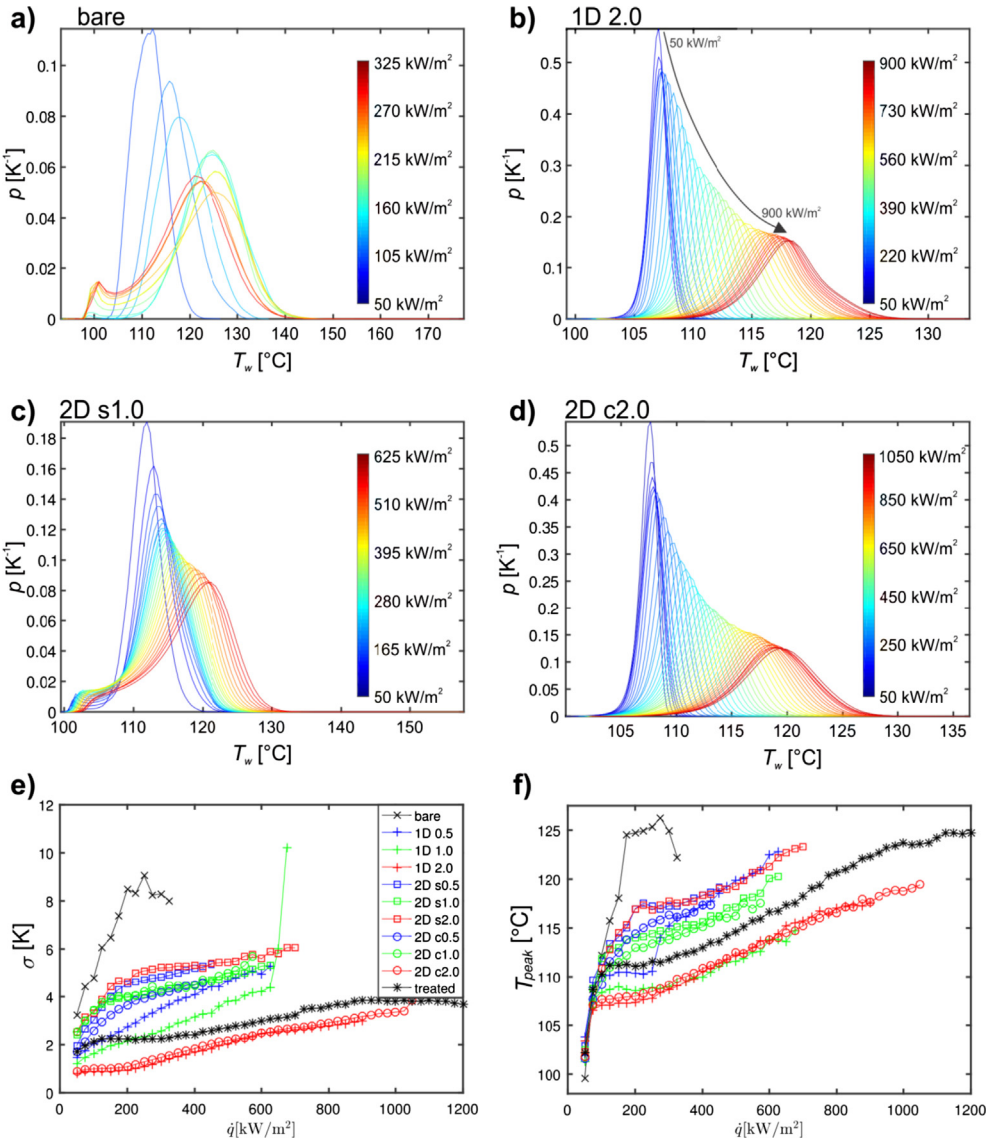

Fig. 5. Heater wall-temperature distributions (a-d); standard deviations of the wall-temperatures (e); and temperatures at the peaks of the heater wall-temperature distributions during saturated pool boiling.

higher than those for the untreated surface. This finding results in lower deviation of the surface temperature. High values of standard deviation for the 1D 1.0 sample at heat flux above 625 kW/m^2 are most likely the consequence of the presence of local dry-outs, which eventually lead to the burnout. The values of temperature at the peaks of the heater wall-temperature distributions [Fig. 5(f)] are similar to the average wall-temperature and are generally increasing with the heat flux.

The most prominent active nucleation sites were identified from the averaged temperature field (from all frames, recorded in 10 s, i.e., from 10,000 frames) at heat flux values of 100 kW/m^2 and 300 kW/m^2 (Figs. 6 and 7), respectively. During nucleate boiling, each nucleating bubble causes a significant temperature drop and therefore colder (blue) regions on the averaged temperature fields represents the most prominent nucleation sites. On bare and fully treated sample [Fig. 6(a–b) and Fig. 7(a–b)] the

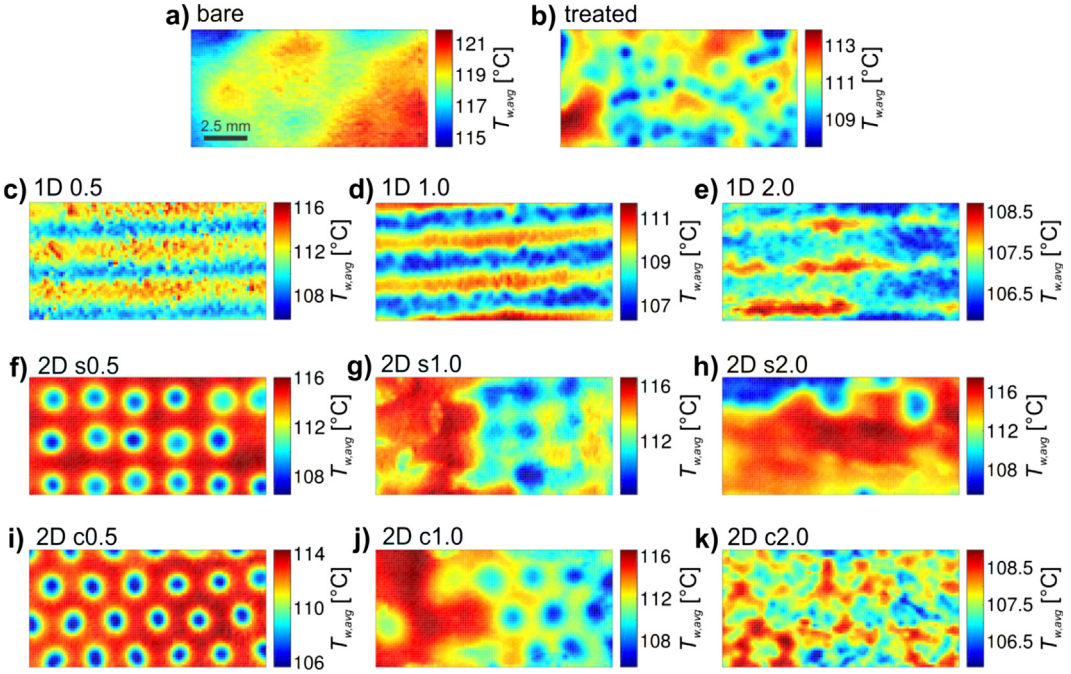

Fig. 6. Time-averaged temperature fields at the heat flux of 100 kW/m^2.

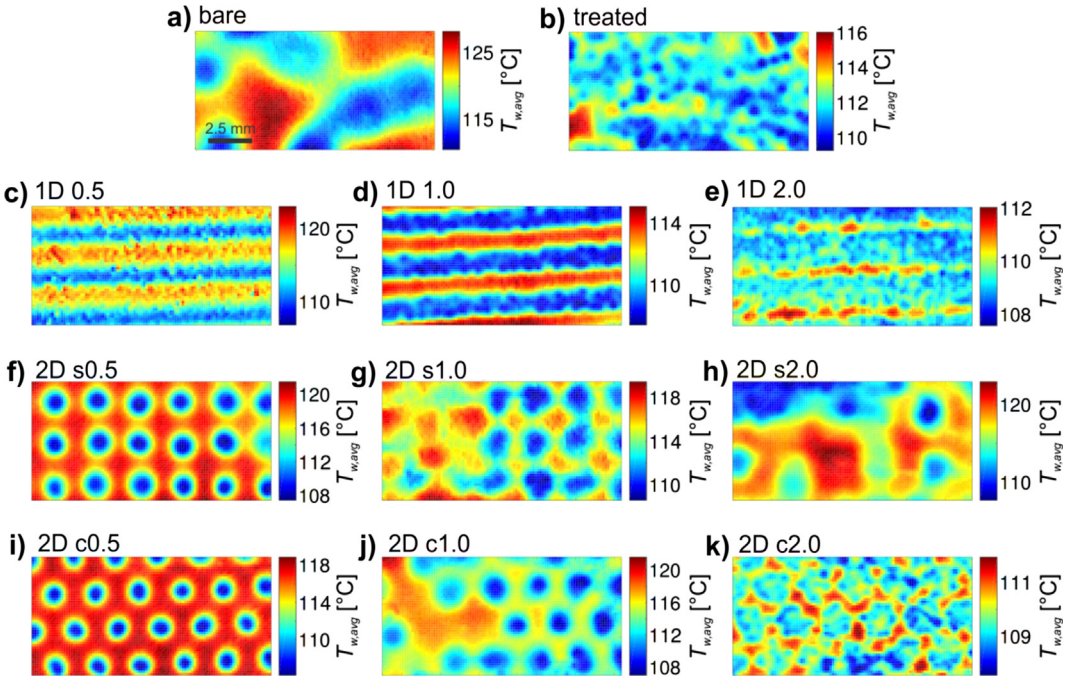

Fig. 7. Time-averaged temperature fields at the heat flux of 300 kW/m^2.

nucleation sites are randomly distributed across entire heater, as already shown by several authors [33,34]. Contrarily, the patterned laser-textured surfaces [Fig. 6(c–k) and Fig. 7(c–k)], lead to controlled nucleate boiling, where the nucleation occurs exclusively on the textured areas. This result is in accordance with our previous experiments [8]. This evidently confirms that laser-made structures promote bubble growth and limit the bubble size, thereby providing a positive effect on heat transfer coefficient. Fabricated μ -cavities effectively trap vapour and provide sites for bubble growth. Note that larger textured areas on 1D and 2D samples with 1 mm and 2 mm features provide several nucleation sites on the same textured region. On 2D s0.5 and 2D c0.5 samples, we detected only one nucleation site on each textured region (possibly because of the limited resolution of the IR camera), resulting in a clearly visible temperature pattern, where each cold spot corresponds to the location of laser-textured region [e.g., see Fig. 6(f,i) and Fig. 7(f,i)]. These two surfaces show the most contrast in time averaged temperature between the nucleation sites and untreated areas, indicating that the nucleation sites does not significantly affect each other. The lowest variation in average temperature field is observed on 1D 2.0 and 2D c2.0 samples, which had the highest HTC.

With increase of the heat flux up to 300 kW/m^2 (Fig. 7), the number of active nucleation sites increases, as was also mathematically evaluated by Wang et al. [35]; this phenomenon is clearly visible on the fully treated sample [Fig. 7(b)]. The increase in heat flux activated more nucleation sites on the sample 2D s2.0. Therefore, the laser-textured regions could be identified based on the average temperature field [Fig. 7(h)].

A custom-made programme code in Matlab was employed for identification and calculation of *(i)* time averaged nucleation frequency, f; *(ii)* bubble activation temperature, T_{act}; and *(iii)* bubble deactivation temperature, T_{dea}. To determine these values, we locally examined individual nucleation sites. The investigated sites were selected from the time-averaged temperature fields (as particular cold region). A nucleation site remains active until bubble growth stops and a bubble departs from the heater surface. Next, the nucleation site becomes inactive and heat removal by quenching and natural convection is resumed [36]. Thus, the activation temperature was identified from the local maxima, whereas the deactivation temperature was identified from as the local minima of the time-dependent temperature signal on the nucleation locations. Fig. 8 depicts the average values of nucleation frequency as well as bubble activation and deactivation temperatures for five selected nucleation sites on each sample (on the bare sample fewer sites were analysed). The nucleation frequency generally increases with increasing heat flux. The lowest nucleation frequencies were measured on the bare sample [Fig. 8(a)] because of the lack of μ -cavities and the resulting high activation temperatures causes relatively large bubbles to grow and detach over a significantly longer period than bubbles formed on laser-textured areas.

The temperature difference between the activation and deactivation temperatures [Fig. 8(b)] is inversely proportional to the nucleation frequency for all samples, with the exception of the bare heater at 100 kW/m^2, which might be a consequence of smaller sample size (only two sites were found and analysed in that case). The average activation and deactivation temperatures [Fig. 8(c and d)] monotonically increase with increasing heat flux on the laser-textured samples, whereas the bare sample indicates a decreasing trend. On the bare sample, the activation temperature remains near 119 °C for all analysed heat flux values, whereas the deactivation temperature drops to close to the saturation temperature; this shows that bubbles on the bare sample are significantly larger than those on the laser-textured samples.

Note that two-dimensional boiling surface designs did not perform better than the one-dimensional ones for every case (Fig. 4). Therefore, prevention of horizontal coalescence of bubbles is clearly not the dominant mechanism for heat transfer enhancement.

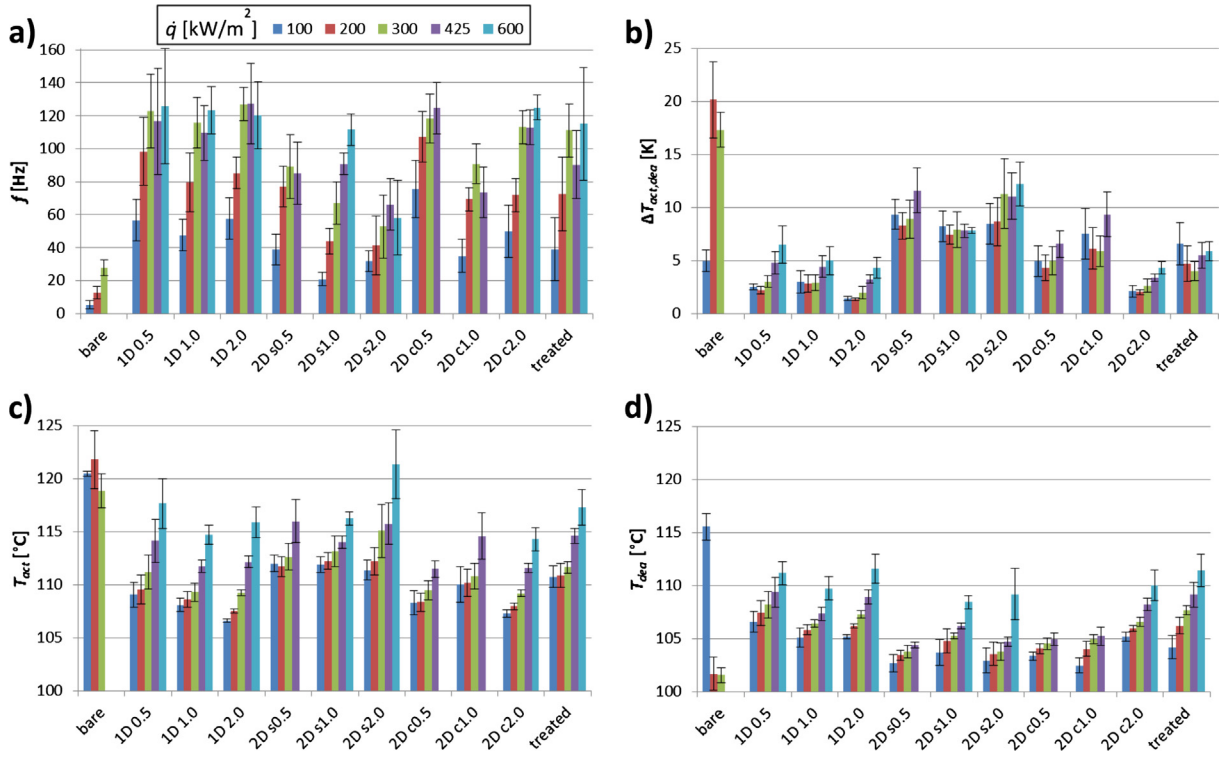

Fig. 8. Average nucleation frequency (a), temperature difference between activation and deactivation temperature (b), activation (c) and deactivation (d) temperature.

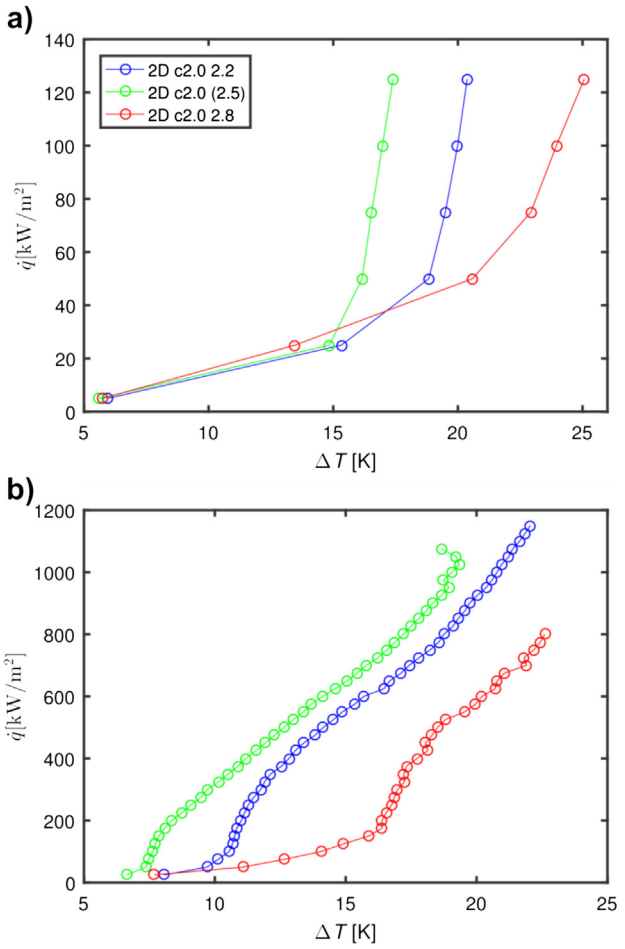

Fig. 9. Boiling curves for subcooled (a) and saturated (b) pool boiling on 2D c2.0 laser-textured patterned surfaces with spacing (A) values equal to 2.2 mm, 2.5 mm and 2.8 mm.

In the last part of our experiments we kept the size of features the same (B = 2.0 mm) and varied the distance (A in Fig. 1) between them as 2.2 mm, 2.5 mm and 2.8 mm. The tests were performed on the boiling surface depicted with 2D c in subcooled (10 K of subcooling) and saturated pool boiling conditions. The boiling curves (Fig. 9) clearly lead to the conclusion that the optimal distance between the laser-textured patterned regions coincides with the capillary length, which is equal to 2.5 mm for saturated water at 1 atm. However, further investigation is still required to test this hypothesis for other working fluids (e.g., alcohols, refrigerants, and dielectrics).

4. Conclusions

The tested surfaces with one- and two-dimensional laser-textured patterns enhanced nucleate water pool boiling heat transfer in both subcooled and saturated conditions. This enhancement is caused by laser texturing of the surfaces, leading to formation of μ-cavities at the surfaces. The μ-cavities effectively trap vapour and provide sites for growth of vapour bubbles (active nucleation sites). Prevention of the coalescence of bubbles was not the dominant mechanism that contributed to the heat transfer enhancement, as confirmed from the results on the 1D 2.0 sample, where the coalescences in the direction of the treated lines were enabled, but the sample still showed the second largest average HTC among all tested surfaces.

The highest measured heat flux prior to burnout (1200 kW/m^2) was achieved on the fully treated sample. The highest HTC (54.6 kW/m^2 K at 1050 kW/m^2), as well as average HTC (37.5 kW/m^2 K), was observed on the 2D c2.0 sample. The highest achieved heat flux (on the treated sample) was increased by factor of 3.7 compared to the bare sample. The 2D c2.0 sample that showed the highest measured HTC provided on average 12 K lower superheating compared to the bare sample in the range from 50 to 325 kW/m^2. The capillary length of the working fluid (water) was experimentally confirmed to be the optimal distance between the laser-textured regions to achieve the highest heat transfer coefficient during pool boiling of water.

Conflicts of Interest Statement

Declarations of interest: none.

Acknowledgements

The authors acknowledge the financial support from the Slovenian Research Agency (research core funding Nos. P2-0223 and P2-0392), the support from the European Space Agency (MAP BOILING (MANBO) project under contract 4200020289), and the support of SPI Lasers Ltd. via the lending of their fiber laser within the research project *Surface functionalization by nanosecond fiber laser texturing* (nsFLaT). The authors thank Dr. Matej Hočevar for the SEM images of laser-textured surfaces taken at the Institute of Metals and Technology in Ljubljana, Slovenia and Dr. Luka Čerče for help with measuring the surface roughness of the samples at Faculty of Mechanical Engineering in Ljubljana, Slovenia.

References

[1] Y. Tian, K. Zhang, N. Wang, Z. Cui, L. Cheng, Numerical study of pool boiling heat transfer in a large-scale confined space, Appl. Therm. Eng. 118 (2017) 188–198.
[2] A. Jaikumar, S.G. Kandlikar, Enhanced pool boiling for electronics cooling using porous fin tops on open microchannels with FC-87, Appl. Therm. Eng. 91 (2015) 426–433.
[3] H.S. Jo, S. An, H.G. Park, M.-W. Kim, S.S. Al-Deyab, S.C. James, J. Choi, S.S. Yoon, Enhancement of critical heat flux and superheat through controlled wettability of cuprous-oxide fractal-like nanotextured surfaces in pool boiling, Int. J. Heat Mass Transf. 107 (2017) 105–111.
[4] K.K. Wong, K.C. Leong, Saturated pool boiling enhancement using porous lattice structures produced by Selective Laser Melting, Int. J. Heat Mass Transf. 121 (2018) 46–63.
[5] A. Jaikumar, S.G. Kandlikar, Ultra-high pool boiling performance and effect of channel width with selectively coated open microchannels, Int. J. Heat Mass Transf. 95 (2016) 795–805.
[6] I. Golobič, M. Zupančič, Wall-temperature distributions of nucleate pool boiling surfaces vs. boiling curves: a new approach, Int. J. Heat Mass Transf. 99 (2016) 541–547.
[7] M. Zupančič, M. Steinbücher, P. Gregorčič, I. Golobič, Enhanced pool-boiling heat transfer on laser-made hydrophobic/superhydrophilic polydimethylsiloxane-silica patterned surfaces, Appl. Therm. Eng. 91 (2015) 288–297.
[8] P. Gregorčič, M. Zupančič, I. Golobič, Scalable surface microstructuring by a fiber laser for controlled nucleate boiling performance of high- and low-surface-tension fluids, Sci. Rep. 8 (1) (2018) 7461.
[9] Y.-Y. Li, Z.-H. Liu, B.-C. Zheng, Experimental study on the saturated pool boiling heat transfer on nano-scale modification surface, Int. J. Heat Mass Transf. 84 (2015) 550–561.
[10] A.R. Betz, J. Jenkins, C.-J.C. Kim, D. Attinger, Boiling heat transfer on superhydrophilic, superhydrophobic, and superbiphilic surfaces, Int. J. Heat Mass Transf. 57 (2) (2013) 733–741.
[11] X. Chen, H. Qiu, Bubble dynamics and heat transfer on a wettability patterned surface, Int. J. Heat Mass Transf. 88 (2015) 544–551.
[12] A. Fazeli, M. Mortazavi, S. Moghaddam, Hierarchical biphilic micro/nanostructures for a new generation phase-change heat sink, Appl. Therm. Eng. 78 (2015) 380–386.
[13] X. Dai, X. Huang, F. Yang, X. Li, J. Sightler, Y. Yang, C. Li, Enhanced nucleate boiling on horizontal hydrophobic-hydrophilic carbon nanotube coatings, Appl. Phys. Lett. 102 (16) (2013) 161605.
[14] M. Yamada, B. Shen, T. Imamura, S. Hidaka, M. Kohno, K. Takahashi, Y. Takata, Enhancement of boiling heat transfer under sub-atmospheric pressures using biphilic surfaces, Int. J. Heat Mass Transf. 115 (2017) 753–762.

[15] M. Zupančič, M. Može, P. Gregorčič, I. Golobič, Nanosecond laser texturing of uniformly and non-uniformly wettable micro structured metal surfaces for enhanced boiling heat transfer, Appl. Surf. Sci. 399 (2017) 480–490.
[16] Y.Y. Hsu, On the size range of active nucleation cavities on a heating surface, J. Heat Transfer 84 (3) (1962) 207–213.
[17] S. Jun, S. Sinha-Ray, A.L. Yarin, Pool boiling on nano-textured surfaces, Int. J. Heat Mass Transf. 62 (2013) 99–111.
[18] E.M. Slomski, S. Fischer, H. Scheerer, M. Oechsner, P. Stephan, Textured CrN thin coatings enhancing heat transfer in nucleate boiling processes, Surf. Coat. Technol. 215 (2013) 465–471.
[19] R.P. Sahu, S. Sinha-Ray, S. Sinha-Ray, A.L. Yarin, Pool boiling on nano-textured surfaces comprised of electrically-assisted supersonically solution-blown, copper-plated nanofibers: experiments and theory, Int. J. Heat Mass Transf. 87 (2015) 521–535.
[20] T.J. Hendricks, S. Krishnan, C. Choi, C.-H. Chang, B. Paul, Enhancement of pool-boiling heat transfer using nanostructured surfaces on aluminum and copper, Int. J. Heat Mass Transf. 53 (15) (2010) 3357–3365.
[21] M.M. Rahman, J. Pollack, M. Mccarthy, Increasing Boiling Heat Transfer using Low Conductivity Materials, Sci. Rep. 5 (2015) 13145.
[22] P. Gregorčič, B. Šetina-Batič, M. Hočevar, Controlling the stainless steel surface wettability by nanosecond direct laser texturing at high fluences, Appl. Phys. A 123 (12) (2017) 766.
[23] J. Petkovsek, Y. Heng, M. Zupancic, H. Gjerkes, F. Cimerman, I. Golobic, IR thermographic investigation of nucleate pool boiling at high heat flux, Int. J. Refrig 61 (2016) 127–139.
[24] A.S. Surtaev, V.S. Serdyukov, M.I. Moiseev, Application of high-speed IR thermography to study boiling of liquids, Instrum. Exp. Tech. 59 (4) (2016) 615–620.
[25] C. Gerardi, J. Buongiorno, L.-W. Hu, T. Mckrell, Measurement of nucleation site density, bubble departure diameter and frequency in pool boiling of water using high-speed infrared and optical cameras, in: V: Boiling 2009: 7 ECI International conference on boiling heat transfer, Brazil, 2009.
[26] G. Mchale, N. Shirtcliffe, M. Newton, Super-hydrophobic and super-wetting surfaces: analytical potential?, Analyst 129 (4) (2004) 284–287
[27] U. Trdan, M. Hočevar, P. Gregorčič, Transition from superhydrophilic to superhydrophobic state of laser textured stainless steel surface and its effect on corrosion resistance, Corros. Sci. 123 (2017) 21–26.
[28] D.V. Ta, A. Dunn, T.J. Wasley, R.W. Kay, J. Stringer, P.J. Smith, C. Connaughton, J. D. Shephard, Nanosecond laser textured superhydrophobic metallic surfaces and their chemical sensing applications, Appl. Surf. Sci. 357 (2015) 248–254.
[29] A.-M. Kietzig, S.G. Hatzikiriakos, P. Englezos, Patterned superhydrophobic metallic surfaces, Langmuir 25 (8) (2009) 4821–4827.
[30] C.C. Hsu, W.C. Chiu, L.S. Kuo, P.H. Chen, Reversed boiling curve phenomenon on surfaces with interlaced wettability, AIP Adv. 4 (10) (2014) 107110.
[31] N. Zuber, Hydrodynamic aspects of boiling heat transfer (thesis), Ramo-Wooldridge Corp., Los Angeles, CA (United States); Univ. of California, Los Angeles, CA (United States), 1959.
[32] I. Golobič, A.E. Bergles, Effects of heater-side factors on the saturated pool boiling critical heat flux, Exp. Therm. Fluid Sci. 15 (1) (1997) 43–51.
[33] R. Judd, N. Balakrishnan, Applicability of statistics and probability theory to nucleate pool boiling heat transfer, Encyclopedia Stat. Sci. (2011), https://doi.org/10.1002/0471667196.ess7147.
[34] K. Wang, S. Gong, B. Bai, W. Ma, On the relation between nucleation site density and critical heat flux of pool boiling, Heat Transfer Eng. (2017) 1–9.
[35] C.H. Wang, V.K. Dhir, Effect of surface wettability on active nucleation site density during pool boiling of water on a vertical surface, J. Heat Transfer 115 (3) (1993) 659–669.
[36] I. Golobič, E. Pavlovič, J. Von Hardenberg, M. Berry, R.A. Nelson, D.B.R. Kenning, L.A. Smith, Comparison of a mechanistic model for nucleate boiling with experimental spatio-temporal data, Chem. Eng. Res. Des. 82(4), 435-444.